Crystal field analysis of Pm^{3+} ($4f^4$) and Sm^{3+} ($4f^5$) and lattice location studies of ^{147}Nd and ^{147}Pm in *w*-AlN

Ulrich Vetter,[1,*] John B. Gruber,[2] Anmol S. Nijjar,[2] Bahram Zandi,[3] Gregor Öhl,[1,*] Ulrich Wahl,[4] Bart De Vries,[5] Hans Hofsäss,[1] Marc Dietrich,[6] and the ISOLDE Collaboration[6]

[1]*2. Physikalisches Institut, Universität Göttingen, Friedrich Hund-Platz 1, 37073 Göttingen, Germany*

[2]*Department of Physics and Astronomy, The University of Texas at San Antonio, San Antonio, Texas 78249-0697, USA*

[3]*ARL/Adelphi Laboratory Center, U.S. Army, Adelphi, Maryland 20783-1197, USA*

[4]*Instituto Tecnológico e Nuclear, Estrada Nacional 10, 2686-953 Sacavém, Portugal*

[5]*Instituut voor Kern- en Stralingsfysica, K. U. Leuven, Celestijnenlaan 200D, 3001 Leuven, Belgium*

[6]*EP Division, CERN, CH-1211 Geneva 23, Switzerland*

(Received 13 June 2006; published 2 November 2006)

We report a detailed crystal field analysis of Pm^{3+} and Sm^{3+} as well as lattice location studies of ^{147}Pm and ^{147}Nd in 2H-aluminum nitride (*w*-AlN). The isotopes of mass 147 were produced by nuclear fission and implanted at an energy of 60 keV. The decay chain of interest in this work is $^{147}Nd \rightarrow {}^{147}Pm \rightarrow {}^{147}Sm$ (stable). Lattice location studies applying the emission channeling technique were carried out using the β^- particles and conversion electrons emitted in the radioactive decay of $^{147}Nd \rightarrow {}^{147}Pm$. The samples were investigated as implanted, and also they were investigated after annealing to temperatures of 873 K as well as 1373 K. The main fraction of about 60% of both ^{147}Pm as well as ^{147}Nd atoms was located on substitutional Al sites in the AlN lattice; the remainder of the ions were located randomly within the AlN lattice. Following radioactive decay of ^{147}Nd, the cathodoluminescence spectra of Pm^{3+} and Sm^{3+} were obtained between 500 nm and 1050 nm at sample temperatures between 12 K and 300 K. High-resolution emission spectra, representing intra-4*f* electron transitions, were analyzed to establish the crystal-field splitting of the energy levels of Sm^{3+} ($4f^5$) and Pm^{3+} ($4f^4$) in cationic sites having C_{3v} symmetry in the AlN lattice. Using crystal-field splitting models, we obtained a rms deviation of 6 cm^{-1} between 31 calculated-to-experimental energy (Stark) levels for Sm^{3+} in AlN. The results are similar to those reported for Sm^{3+} implanted into GaN. Using a set of crystal-field splitting parameters B_{nm}, for Pm^{3+} derived from the present Sm^{3+} analysis, we calculated the splitting for the $^5F_1$, $^5I_4$, and $^5I_5$ multiplet manifolds in Pm^{3+} and obtained good agreement between the calculated and the experimental Stark levels. Temperature-dependent lifetime measurements are also reported for the emitting levels $^4F_{5/2}$ (Sm^{3+}) and $^5F_1$ (Pm^{3+}).

DOI: 10.1103/PhysRevB.74.205201 PACS number(s): 78.40.Fy, 78.60.Hk, 71.70.Ch

I. INTRODUCTION

Radiative intra-4*f* electron transitions of triply ionized lanthanide ions (Ln^{3+}) doped into very wide band gap semiconductors such as 2H-aluminum nitride (*w*-AlN) reveal high potential for optoelectronic applications from the near infrared to the near ultraviolet region of the electromagnetic spectrum.[1–7] The main results in the luminescence spectra compared to Ln^{3+}-doped *w*-GaN is the excellent suitability of $AlN:Tm^{3+}$ as a blue-light emitter at around 468 nm (Ref. 8) and the ultraviolet emission of $AlN:Gd^{3+}$ at around 318 nm.[5,7] By using the ternary compound $Al_xGa_{1-x}N$, which allows for a wide range in the choice of the band gap, modification of the light emission of a certain lanthanide ion is possible to some extent.[9,10] Regarding the very wide band gap of *w*-AlN, an equivalently attractive but more difficult to handle host matrix is the III-V semiconductor cubic boron nitride, for which doping with lanthanides and successful activation of Ln^{3+}-related luminescence has been demonstrated for both ion implantation[11] and doping during growth.[12,13]

For Ln^{3+} in GaN light emission due to radiative intra-4*f* electron transitions of the complete lanthanide series has been demonstrated successfully; the only exceptions are given by Ce^{3+} and Pm^{3+}. In the case of Ce^{3+}, the single $^2F_{7/2} \rightarrow {}^2F_{5/2}$ multiplet-to-multiplet transition lies within the far infrared region, and radiative $5d \rightarrow 4f$ transitions of Ce^{3+} that would lead to visible light emission have not been demonstrated in semiconductors. Optical investigations of Pm^{3+} in semiconductor host matrices have, to our best knowledge, not been performed so far due to the problems associated with radioactive isotopes, although the diffusion behavior of Pm in silicon was already studied in the past.[14] The choice of promethium, for which no stable isotope exists, is therefore motivated by interest in the spectroscopic properties associated with the trivalent ion. Combining ion implantation into semiconductors and cathodoluminescence (CL) measurements of Pm^{3+} is very attractive in this case because the overall number of radioactive atoms in a sample can be limited to less than 10^{11} ions.

While the radioactivity of promethium poses environmental problems for its use in technology, its spectroscopic properties were examined in the past when interest arose concerning its potential for stimulated emission as Pm^{3+} doped into materials having favorable optical and mechanical properties. A detailed crystal-field splitting analysis of the energy levels of $Pm^{3+}:LaCl_3$ has been reported that includes earlier references to spectroscopic studies of Pm^{3+} in other hosts.[15]

In this work we combine lattice location studies and crystal-field calculations using radioactive isotopes. We re-

port lattice location studies of ^{147}Pm and ^{147}Nd as well as crystal-field calculations based on an analysis of CL spectra of Pm^{3+} and Sm^{3+} in initially mainly ^{147}Nd-implanted 2H-aluminum nitride. The subsequent decay of ^{147}Pm to stable ^{147}Sm allows us to compare our spectroscopic data to earlier crystal-field investigations of Sm^{3+} in GaN.[16]

II. EXPERIMENTAL DETAILS

Films of AlN, grown on Al_2O_3 substrates by metal-organic chemical vapor deposition, were obtained from commercial sources. The thicknesses of these AlN films were determined by Rutherford backscattering (RBS) to 400 Å. The substrate was cut into small pieces of approximately 5×5 mm^2 and cleaned prior to implantation.

Radioactive isotopes were implanted at an energy of 60 keV and fluences of approximately 1×10^{13} ions/cm^2 (aperture diameter: 1 mm) at the online isotope separator ISOLDE (Ref. 17) at CERN. The ions were produced by bombardment of a UC_2 target with high-energetic protons and mass separated using the local general purpose mass separator (GPS). The samples were tilted by approx. 10° during implantation in order to avoid channeling of the incident ions. The final samples at hand contained a mixture of mainly neutron-rich isotopes of mass 147, with the short-life isotopes rapidly decaying to ^{147}Nd. The final decay chain of interest to us for the experiments in this work is

$$^{147}\mathrm{Nd} \xrightarrow[Q_{\beta^-}=896.1\ \mathrm{keV}]{t_{1/2}=10.96d} {}^{147}\mathrm{Pm} \xrightarrow[Q_{\beta^-}=224.1\ \mathrm{keV}]{t_{1/2}=2.62y} {}^{147}\mathrm{Sm}.$$

Both ^{147}Nd and ^{147}Pm decay via β^- decay with the Q factors and half-lifes as indicated.[18] ^{147}Pm is the isotope with the longest half-life of all unstable isotopes of mass 147. This fact is important regarding the luminescence measurements, because we simply need to wait a sufficiently long time in order to be sure that only ^{147}Pm and its stable daughter isotope ^{147}Sm remain in the sample.

Emission channeling[19,20] spectra were taken by mounting the samples under vacuum conditions on a two-axes goniometer. The emitted β^- particles and conversion electrons at room temperature were observed with a two-dimensional electron detector setup.[21,22] For lattice location studies both the β^- particles in the energy range above 95 keV as well as the 45.9 keV K-conversion electrons of ^{147}Pm emitted in the decay, $^{147}\mathrm{Nd}\rightarrow{}^{147}$Pm were used for lattice location studies of ^{147}Nd and ^{147}Pm respectively. These charged particles are recorded simultaneously, and discrimination is possible by choosing appropriate energy windows in the later analysis. Emission channeling patterns were recorded around several axes, which allowed us to distinguish between many sites as a matter of their differing geometrical projections onto the planes perpendicular to these axes. In order to study the lattice location of the ions after annealing the samples at higher temperatures, the samples were heated under vacuum conditions to 873 K and 1373 K in quartz ampoules. Emission channeling spectra were recorded after cooling the samples down to room temperature. These two-dimensional electron intensity spectra were fitted against theoretical simulations based on the dynamical theory of electron diffraction.[19,20] An overview on recent emission channeling experiments on ion implanted wide band gap semiconductors is given in Ref. 23.

Another set of samples was implanted in an identical manner and stored for several months to ensure that only ^{147}Sm and ^{147}Pm atoms were present in the samples. At this stage the activity of a single sample was already less than 500 Bq. Shortly before performing the CL measurements, the samples were heated to 1373 K for 30 min under vacuum conditions (below 10^{-6} mbar) in a ceramic tube furnace. The vacuum conditions prohibit contamination of the samples with Cr^{3+} ions that we typically found when combining Al_2O_3 ceramics oven tubes and nitrogen as a flow gas. The annealing temperature of 1373 K, already chosen in our earlier investigations, lies within a temperature range of approximately 1300 K and 1500 K where CL is clearly visible but neither degradation of the sample (measured by, e.g., x-ray diffraction spectroscopy) nor diffusion of the implanted ions (measured by RBS) significantly starts to take place. An alternative approach to recover samples from implantation damage would be laser annealing.[24]

CL spectra were recorded with a spectrograph, charge-coupled device (CCD) camera and photomultiplier, the same setup that we used in our earlier crystal field-investigations.[25,26] Survey spectra as well as high-resolution CL spectra were taken with the CCD camera and were not corrected for the response function of the setup. The positions of lines corresponding to transitions between individual Stark levels are mainly extracted from the luminescence spectra by identifying minima in the second derivative of the spectra. Time-resolved CL spectra were performed by pulsing the electron beam; the photons were monitored with photomultiplier and multichannel scaler in this case.

III. LATTICE LOCATION STUDIES

Lattice location experiments in AlN suffer from the fact that even the best quality thin films that are currently available are not perfect single crystals but consist of single-crystalline micrometer-sized domains that are slightly misoriented with respect to each other and separated by dislocation-rich regions. The approximate size (0.1–1 μm) and spread in the orientation (around 0.2° tilt and 1.2° twist) of the domains with respect to the average c-axis direction can be characterized by x-ray diffraction measurements, which will be addressed in more detail in a forthcoming publication.[27] Due to the mosaic spread, the experimental channeling patterns represent a superposition of the channeling effects within the single-crystal domains, resulting in angular resolution values of the patterns that are worse than for a perfect single crystal and also depend on the inclination angle towards the c-axis. In our analysis, this deterioration of angular resolution was taken into account by folding the theoretical patterns with appropriate resolution functions. As a consequence of the mosaic spread and the resulting loss of angular resolution, our lattice location results in AlN are less precise than, e.g., in the case of GaN samples, which are available in better quality than AlN films.

Figure 1 (left column) shows experimental emission channeling spectra of β^- particles arising in the decay ^{147}Nd

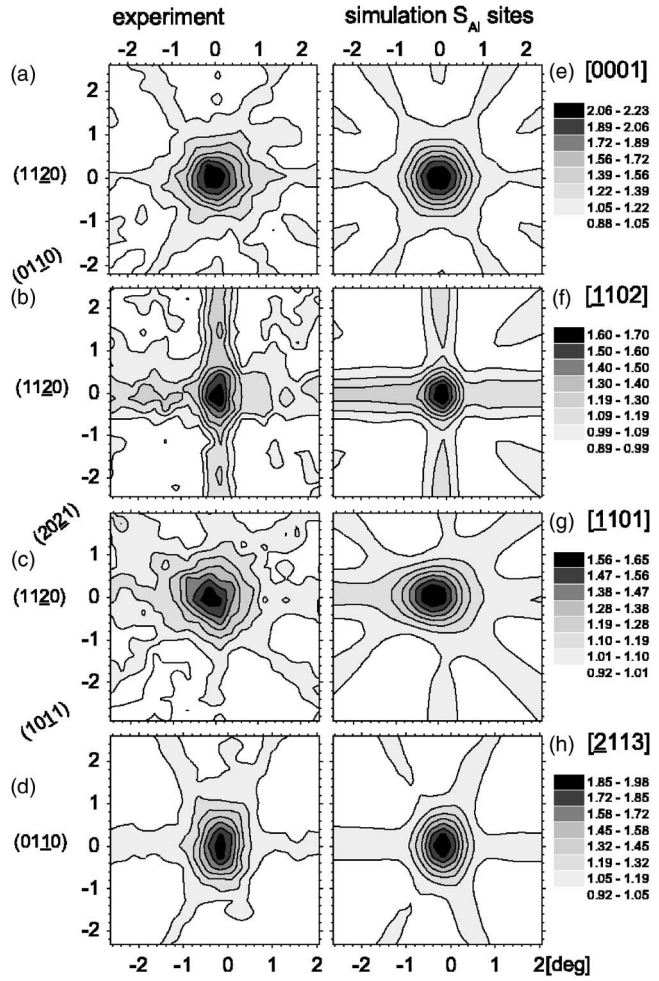

FIG. 1. Experimental emission channeling spectra of the β^- particles arising in the decay $^{147}Nd \rightarrow {}^{147}Pm$ (left) and corresponding simulations for 56(6)% of the ^{147}Nd atoms on substitutional Al sites (right) in the *w*-AlN lattice; the remainder of the ions is located on random sites.

$\rightarrow {}^{147}Pm$, recorded around the [0001], [1102], [1101] and [2113] axes in 2H-AlN, measured as implanted at room temperature. The electron yields are normalized and displayed in grayscaled contour plots; planes are indicated in parentheses. Figure 1 (right column) shows the corresponding simulation assuming 56(6)% of ^{147}Nd atoms on substitutional Al sites in the 2H-AlN lattice. The remainder of the ions are located on random sites in the AlN lattice. Annealing the samples to temperatures of 873 K and 1373 K yielded fractions of 58(5)% and 56(7)% of the ^{147}Nd atoms on substitutional Al sites. In the same manner, lattice location studies of ^{147}Pm were performed monitoring the *K* electrons of ^{147}Pm in the same decay. In this case the experimental spectra are best fitted by assuming fractions of 51(11)% (as implanted), 58(8)% (873 K), and 44(6)% (1373 K) of the ^{147}Pm emitter atoms on substitutional Al sites. The decrease of the substitutional fraction of ^{147}Pm emitter atoms on Al sites at 1373 K is attributed to surface degradation, whose effect on the electron yield is more dominant for low-energetic electrons and cannot be taken into account in the simulations.

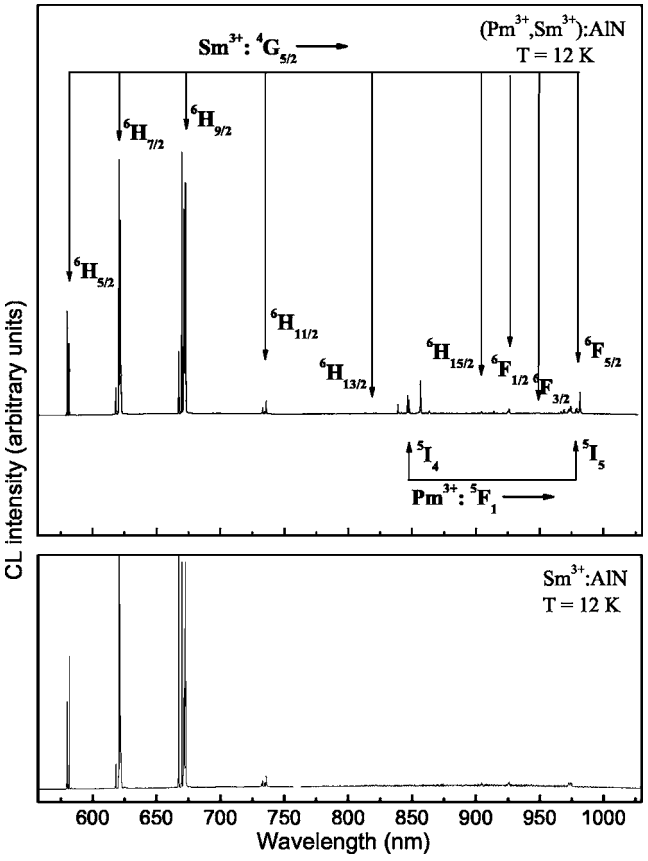

FIG. 2. Cathodoluminescence survey spectra of Sm^{3+}/Pm^{3+} implanted AlN (upper graph) and Sm^{3+} implanted AlN (lower graph), taken at 12 K. The samples were annealed at 1373 K and 1473 K under vacuum conditions. The spectra are not corrected for the response function of the setup.

Diffusion of the ions as the origin can be excluded at such annealing temperatures, as shown by RBS taken from Sm^{3+}—implanted samples that were treated under similar conditions.[28]

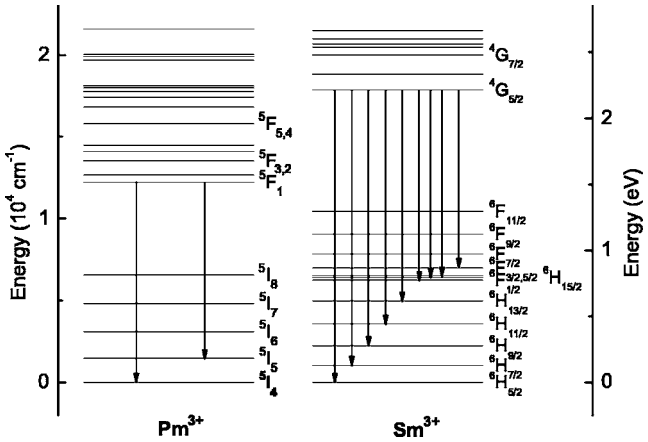

FIG. 3. Calculated energy level diagram for Sm^{3+} and Pm^{3+}, cut at approximately 22 000 cm^{-1}, and observed transitions in the AlN host. The energies of both ions' ground states are arbitrarily set to zero.

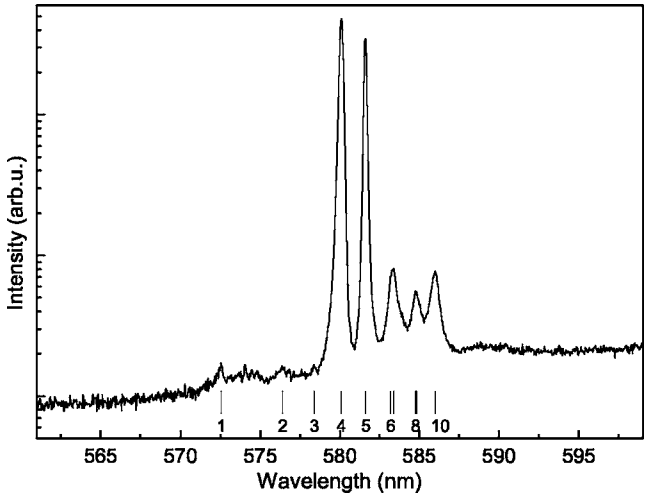

FIG. 4. CL spectrum of the $^4G_{5/2} \rightarrow {}^6H_{5/2}$ transition of Sm^{3+} in *w*-AlN, recorded at 12 K.

IV. OBSERVED LUMINESCENCE SPECTRA

Figure 2 shows the CL survey scans for both a Sm^{3+}/Pm^{3+}-containing 2H-AlN sample taken at 12 K and a second 2H-AlN sample at 12 K which was implanted with stable Sm and annealed under similar conditions as in the case of the radioactive sample. This comparison allows us to identify multiplet-to-multiplet transitions related to Pm^{3+} easier. Both spectra show a dominant red emission in the wavelength range 575 nm to 675 nm. The main differences are observed in the near infrared region between 825 nm and 1000 nm, where the sample containing additionally Pm^{3+} shows a larger number of sharp lines. In order to assign the observed group of lines to transitions between initial and final 4*f*-multiplet manifolds for both Pm^{3+} and Sm^{3+}, we used the computed energy level diagrams shown in Fig. 3. The diagrams are cut at an energy of approximately 22 000 cm^{-1}. We state that the energetic positions of the ions' ground states are neither aligned to each other nor are they aligned to the top of the valence band in *w*-AlN.[29] The assignment is fairly straightforward for both ions, especially since the huge number of closely spaced energy levels above 20 000 cm^{-1} (not shown here) will not give rise to any luminescence because these levels decay nonradiatively to levels lower in energy. They may, on the other hand, be involved in the excitation process. In the case of Sm^{3+}, we are also guided by earlier investigations of Sm^{3+} in GaN.[16] Transitions $^4G_{5/2} \rightarrow {}^6H_{5/2,7/2,9/2,11/2,13/2,15/2}$ and $^4G_{5/2} \rightarrow {}^6F_{3/2,5/2}$ at 12 K are identified in the high-resolution spectra, but some of them are very weak, which explains their absence in the survey scan. In the case of Pm^{3+}, two multiplet-to-multiplet transitions $^5F_1 \rightarrow {}^5I_{4,5}$ are clearly identified in the region that is covered by the measurements. The $^5F_1 \rightarrow {}^5I_5$ transition of Pm^{3+} overlaps the $^4G_{5/2} \rightarrow {}^6F_{5/2}$ transition of Sm^{3+}.

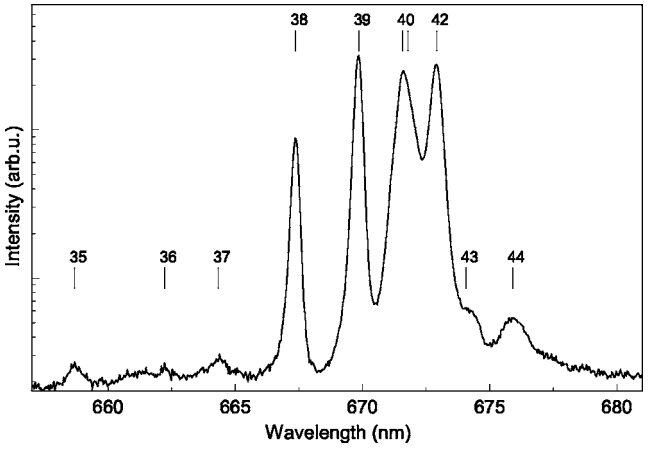

FIG. 6. CL spectrum of the $^4G_{5/2} \rightarrow {}^6H_{9/2}$ transition of Sm^{3+} in *w*-AlN, recorded at 12 K.

Examples of high-resolution CL spectra obtained at 12 K for Sm^{3+} are shown in Figs. 4–7. These spectra represent electronic transitions from the $^4G_{5/2}$ manifold to the ground state, $^6H_{5/2}$ (Fig. 4) and to excited manifolds $^6H_{7/2}$, $^6H_{9/2}$, and $^6H_{11/2}$ (Figs. 5–7). The characteristic red fluorescence from $^4G_{5/2}$ to the ^6H_J multiplets has been analyzed for Sm^{3+} in a number of host crystals and glasses.[30] The emitting Stark level in $^4G_{5/2}$ in Sm^{3+}:GaN is reported at 17 280 cm^{-1}.[16] Taking peak 4 in Fig. 4 listed in Table I (580.11 nm, 17 233 cm^{-1}) as the transition from the lowest energy Stark

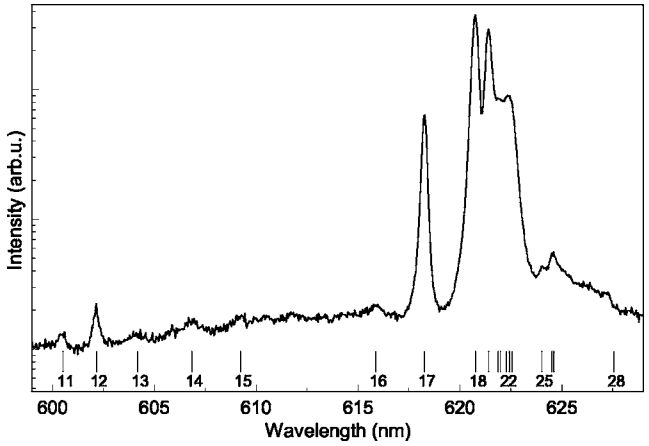

FIG. 5. CL spectrum of the $^4G_{5/2} \rightarrow {}^6H_{7/2}$ transition of Sm^{3+} in *w*-AlN, recorded at 12 K.

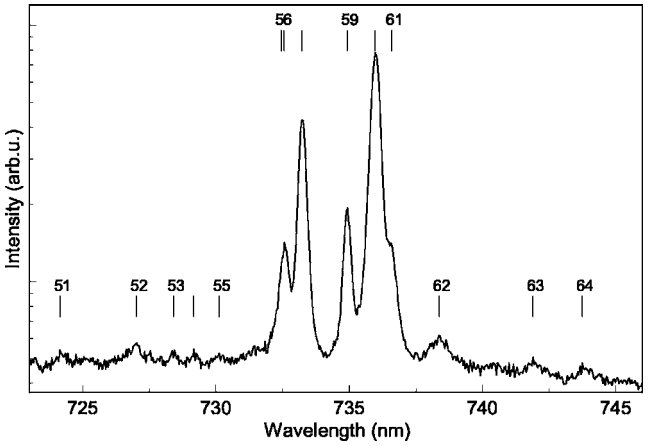

FIG. 7. CL spectrum of the $^4G_{5/2} \rightarrow {}^6H_{11/2}$ transition of Sm^{3+} in *w*-AlN, recorded at 12 K.

TABLE I. Emission from the $^4G_{5/2}$ Stark level at 17 233 cm^{-1} to the ^6H_J and ^6F_J manifolds in $Sm^{3+}(4f^5)$.[a]

$^{2S+1}L_J$[b]	Trans.[c]	λ (nm)[d]	E (cm^{-1})[e]	ΔE (cm^{-1})[f]	E (cm^{-1})[g]	E (calc)[h]	μ
$^6H_{5/2}$	4	580.11	17233	0	0	0	±1/2
(59)	5	581.6	17189	44	42	34	±1/2
	6	583.18	17143	90	83	95	±3/2
	9	584.82	17095				
	10	586.01	17060				
$^6H_{7/2}$	17	618.25	16170	1063	1067	1065	±1/2
(1153)	18	620.76	16105	1128	1143	1128	+/2
	19	621.4	16088				
	22	622.27	16066				
	23	622.42	16062	1171	1175	1165	±1/2
	26	624.5(b)	16008	1225	1223	1227	±3/2
	27	626.6(b)	16006				
	28	627.5(b)	15932				
$^6H_{9/2}$	38	667.37	14980	2253	2264	2258	±1/2
(2346)	39	669.85	14925	2308	2293	2318	±1/2
	40	671.57	14887	2346	2336	2342	±3/2
	41	672.8(sh)	14860				
	42	672.91	14858	2375	2364	2386	±1/2
	43	674.07	14831	2402	2395	2394	±3/2
	44	675.9(b)	14791				
$^6H_{11/2}$	57	732.57	13647	3586		3577	±3/2
(3644)	58	733.22	13635	3598	3611	3592	±1/2
	59	734.93	13603	3630	3630	3629	±1/2
	60	735.97	13584	3649		3658	±3/2
	61	736.61	13572	3661	3660	3667	±1/2
	62	738.37	13540	3693		3698	±1/2
$^6H_{13/2}$	65	813.34	12292	4941	4925	4944	±1/2
(5010)	66	814.02	12281	4952	4940	4948	±1/2
	67	815(b)	12267	4966		4975	±3/2
	67(a)	817(b)	12237	4996	4970	4996	±1/2
	67(b)	819(b)	12207	5026		5039	±3/2
	67(c)	819.5	12199	5034	5020	5043	±3/2
	68	821.9(b)	12164	5069	5048	5065	±1/2
$^6H_{15/2}$	96	904.91	11048	6185	6183	6182	±3/2
(6490)	96(a)		10990	6243	6242	6244	±1/2
	97	914.41	10933	6300	6318	6283	±1/2
$^6F_{1/2}$	102	925.54	10802	6431	6425	6436	±1/2
(6427)	105	926.39	10792	6441	6434	6439	±3/2
	105(a)	934.2	10701	6532	6529	6520	±1/2
					6556	6559	±1/2
$^6F_{3/2}$	116	948.2	10543	6690	6670	6686	±1/2
(6689)				6690	6670	6687	±3/2
$^6F_{5/2}$	118	972.64	10279	6954	6952	6956	±3/2

TABLE I. (*Continued.*)

$^{2S+1}L_J$[b]	Trans.[c]	λ (nm)[d]	E (cm^{-1})[e]	ΔE (cm^{-1})[f]	E (cm^{-1})[g]	E (calc)[h]	μ
(6958)	126	975.19	10252	6981	6978	6984	±1/2
	132	977.3	10230	7003	6990	7002	±1/2

[a]CL spectrum of Sm^{3+}:AlN obtained at 12 K.
[b]Terminal multiplet manifold; number in parenthesis is calculated centroid.
[c]Transition label appearing in figures and identified in text.
[d]Emission wavelength in nanometers; sh denotes shoulder; b denotes broad.
[e]Energy of transition in vacuum wave numbers.
[f]Energy difference between emitting and terminal Stark levels.
[g]Energy level (Stark) splitting of comparable manifolds of Sm^{3+} in GaN (Ref. 16).
[h]Calculated splitting of Sm^{3+} energy levels in cationic sites of C_{3v} symmetry in AlN; B_{nm} listed in Table III.

level in $^4G_{5/2}$ to the ground-state Stark level, we can analyze the experimental crystal-field splitting of the ^6H_J, ^6F_J multiplets as given in Table I. Other transitions numbered in Figs. 4–7 are listed in column 2 of Table I. Our modeling calculations predict the emitting Stark level at 17 230 cm^{-1}, which agrees well with the energy of the transition represented by peak 4.

The experimental manifold splitting obtained for Sm^{3+} in AlN (Table I, column 5) can be compared to the splitting scheme reported for Sm^{3+} implanted into GaN (Table I, column 6). The similarity between the two schemes is not unexpected given that the majority of the Sm^{3+} ions occupy cationic sites in GaN and AlN, where the site symmetry is C_3 in both cases given that no defects exist in the vicinity of the ions. Both nitrides have the hexagonal structure with the space group C_{6V}^4-$P6_3$ and lattice constant ratios, c/a, of 1.601 for AlN and 1.625 for GaN. The similarity in manifold splittings has allowed us to use the crystal-field parameters, B_{nm} reported for Sm^{3+}:GaN as the starting set for the crystal-field analysis carried out in the present investigation.

Overlap of Sm^{3+} and Pm^{3+} spectra for some multiplet-to-multiplet transitions complicate the extension of any analysis of the spectra of either ion, which we will address later in more detail. In Table I there is some overlap in spectra representing $^6F_{5/2}$ (Sm^{3+}) and $^5I_5$ (Pm^{3+}), but the remainder of the spectra and analysis in the table are associated only with Sm^{3+} transitions. In Figs. 4–7 very weak, usually broad peaks are observed, which may be due to ions in interstitial sites. Somewhat stronger emission peaks such as 9, 10 (Fig. 4) and 18 and 22 (Fig. 5) for example may involve transitions between Stark levels for Sm^{3+} ions in sites of comparable symmetry not necessarily at cationic sites. However, with the Sm^{3+}:GaN spectra and analysis as a guide, we have chosen an energy level scheme in Table I that represents the most likely set of Stark levels for Sm^{3+} ions in similar cationic sites in AlN.

Since no combinations of energy differences appear in the Sm^{3+} energy-level scheme (Fig. 3) that explain the CL spectra observed between 830 and 870 nm (Fig. 8) and corresponding transitions are absent in the sample containing only Sm^{3+} (Fig. 2), we consider these spectra as possible transitions from the $^5F_1$ manifold to the $^5I_4$, the ground-state manifold of $Pm^{3+}(4f^4)$. In Pm^{3+}:$LaCl_3$ similar emission is observed near 820 nm as transitions between these two manifolds.[31] In the chloride host, a crystal also having hexagonal symmetry, the $^5F_1$ manifold splits into two levels, a doublet and a singlet, at 12 334 cm^{-1} and 12 350 cm^{-1}.[15,32] This splitting is relatively small so that at temperatures above 80 K emission is observed from both Stark levels due to a Boltzmann distribution population. In the present study, Pm^{3+} is assumed to occupy sites of C_{3v} symmetry. The $^5F_1$ manifold also splits into two Stark levels, a doublet and a singlet. From an analysis of the temperature-dependent CL spectra shown in Fig. 8, we identify peaks 72 and 73 as transitions to the ground-state Stark level from the $^5F_1$ manifold having Stark levels at 11 948 cm^{-1} and 11 913 cm^{-1}. Table II provides a detailed listing of the emission peaks. The splitting of the $^5I_4$ manifold is confirmed by transitions from both components of the $^5F_1$ manifold. While the expected number of Stark levels for each multiplet manifold is identified, we cannot experimentally assign degeneracies expected for some Stark levels in C_{3v} symmetry. Traditional polarization and Zeeman studies are not possible given the experimental methods and sample preparation used in these studies.

An example of overlapping Sm^{3+} and Pm^{3+} CL spectra is shown in Fig. 9, representing transitions between $^4G_{5/2} \rightarrow {}^6F_{5/2}$ (Sm^{3+}) and $^5F_1 \rightarrow {}^5I_5$ (Pm^{3+}), obtained between

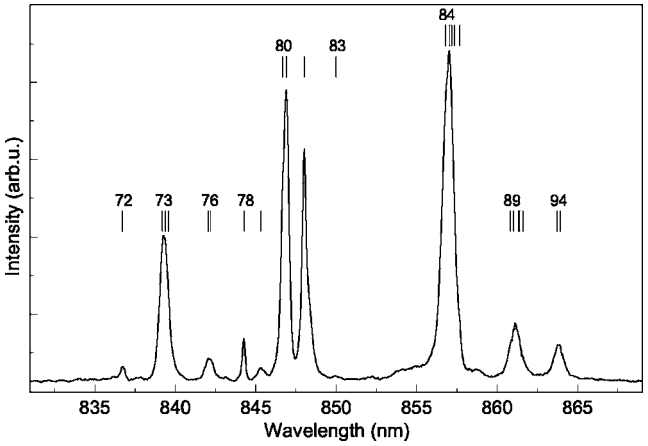

FIG. 8. CL spectrum of the $^5F_1 \rightarrow {}^5I_4$ transition of Pm^{3+} in *w*-AlN, recorded at 12 K.

TABLE II. Emission from $^5F_1$ Stark levels at 11 948 cm^{-1} and 11 918 cm^{-1} to the $^5I_4$ and $^5I_5$ manifolds in $Pm^{3+}(4f^4)$.[a]

$^{2S+1}L_J$[b]	Trans.[c]	λ (nm)[d]	E (cm^{-1})[e]	ΔE (cm^{-1})[f]	E (calc)[g]	μ[h]
$^5I_4$	72	836.71	11948	0	5	0
(211)	73	839.2	11913	0	5	0
	75	839.58	11907	41	36	±1
	76	842.06	11872	41	36	±1
	78	844.28	11843	105	98	0
	80	846.64	11808	105	98	0
	79	845.29	11825	123	122	0
	82	848.01	11789	124	122	0
	83a	854 (sh)	11703	245	239	±1
	84	856.78	11668	245	239	±1
	90	861.01	11611	337	350	±1
	94	863.74	11574	339	350	±1
$^5I_5$	106	961.85	10394	1519	1526	±1
(1619)	107	963.05	10381	1567	1565	0
	109	966.14	10347	1566	1565	0
	108	964.52	10365	1583	1591	±1
	114	967.8	10329	1584	1591	±1
	111	966.74	10341	1607	1611	+1
	116	969.8	10308	1605	1611	+1
	115	968.18	10326	1622	1624	0
	122	979.87	10266	1682	1686	0
	131	976.89	10230	1683	1686	0
	136	979.89	10211	1737	1725	±1
	145	989.24	10178	1735	1725	±1

[a]CL spectrum of Pm^{3+}:AlN obtained at 12 K.
[b]Terminal manifold; number in parentheses is calculated centroid.
[c]Transition label appearing in figures and identified in text.
[d]Emission wavelength in nanometers; sh denotes shoulder.
[e]Energy of transition in vacuum wave numbers.
[f]Energy difference between emitting and terminal Stark levels.
[g]Calculated splitting using B_{nm} reported in Table III for Pm^{3+}.
[h]Predicted crystal quantum number in C_{3v} symmetry; (0) nondegenerate, ±1 twofold degenerate.

960 nm and 990 nm. For Sm^{3+}:GaN, emission from $^4G_{5/2}$ to $^6F_{5/2}$ is observed between 965 nm and 975 nm. Assuming the $^5F_1$ assignment made earlier, the CL spectra appearing in Fig. 9 give terminal levels whose energies are similar to the Stark levels reported for $^5I_5$ in Pm^{3+}:$LaCl_3$.[32] Since the CL spectra in Fig. 9 clearly involve more transitions that can be accounted for assuming Sm^{3+} levels alone, we propose energy difference patterns based on the assumption of overlapping spectra. The analysis of the spectra is represented by the transitions reported in Table I (Sm^{3+}) and Table II (Pm^{3+}). These assignments provide a Stark splitting for the $^6F_{5/2}$ and $^5I_5$ manifolds that is in reasonable agreement with calculated values.

V. CRYSTAL-FIELD SPLITTING CALCULATIONS

We have reported in the past details describing the models used to predict the crystal-field splitting of the energy levels

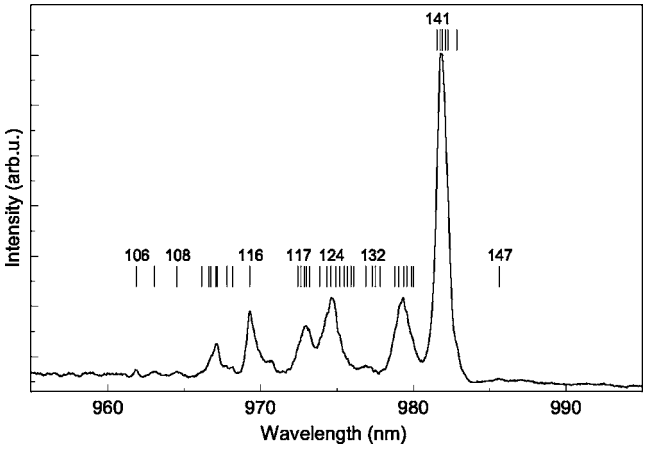

FIG. 9. CL spectrum of the $^5F_1 \rightarrow {}^5I_5$ transition of Pm^{3+} in w-AlN, recorded at 12 K.

of trivalent rare earth ions implanted into the lattice of GaN (Refs. 16, 33, and 34) and AlN.[25,26] A point-charge lattice-sum model that includes structural parameters and ion polarizabilities obtained from literature sources is used to calculate a set of lattice-sum components A_{nm} appropriate to the cationic sites in the lattice. These components are then corrected for shielding and scaling factors that account for the expansion of the radial part of the $4f$ free-ion wave function of the rare earth ion immersed in the nitride lattice. These correction terms described in the earlier work of Morrison *et al.*[35] lead to a set of crystal-field splitting parameters, B_{nm}, that become a starting set for modeling the crystal field splitting of the $^{2S+1}L_J$ multiplet manifolds reported in Tables I and II.

The B_{nm} parameters appear in a crystal-field Hamiltonian that is expressed as

$$H_{CF} = \sum_{n\ even} \sum_{m=-n}^{n} B_{nm}^{*} \sum_{i=1}^{N} C_{nm}(\vec{r}_i), \tag{1}$$

where the normalized one-electron operators transform like the spherical harmonics, where $n=2$, 4, and 6 with $m=0$, ±3, ±6, for $|m| \leq n$ (C_{3v} symmetry). The sum on i runs over 4 for Pm^{3+}($4f^4$) and 5 for Sm^{3+}($4f^5$). Equation (1) is diagonalized together with a parameterized free-ion Hamiltonian that includes Coulombic, spin-orbit, and interconfigurational interaction terms for Pm^{3+} and Sm^{3+} respectively. Our choice for these parameters comes from earlier spectroscopic studies on these ions by Carnall *et al.*[15] The set of eigenvectors was truncated for Sm^{3+} to include only the ^6H_J, ^6F_J,^4G_J, ^4F_J states, and for Pm^{3+}, only the ^5I_J, ^5F_J, $^5S_2$, and the ^3K_J states.

Starting from a set of B_{nm} parameters obtained from the lattice-sum calculations for Sm^{3+}:GaN, Gruber *et al.* determined a set of B_{nm} with a final rms deviation of 7 cm^{-1} between 30 calculated-to-experimental Stark levels.[16] Because a similar splitting is observed in Sm^{3+}:AlN, this set became the starting set for calculating the splitting of the energy levels of Sm^{3+} in AlN for cationic sites having C_{3v} symmetry. From a least-squares fitting analysis of the experimental Stark levels reported in Table I, a final set of B_{nm} parameters was obtained with a rms deviation of 6 cm^{-1} be-

TABLE III. Crystal-field splitting parameters, B_{nm}, for Sm^{3+} and Pm^{3+} in AlN.[a]

B_{nm}	Sm^{3+}:GaN	Sm^{3+}:AlN	Pm^{3+}:AlN
B_{20}	−48.9	−34.1	−203
B_{40}	−860.7	−1036	−866
B_{43}	−321.9	−280.7	−939
B_{60}	692.7	752.3	1339
B_{63}	−265.7	−130.7	−620
B_{66}	261.8	234.8	447

[a]Energy in units of cm^{-1}.

tween 31 calculated-to-experimental Stark levels. Table I compares the experimental data for Sm^{3+} in AlN and GaN with the calculated splitting obtained for Sm^{3+} in AlN. Table III lists the final set of B_{nm} for Sm^{3+} in AlN and GaN.

Table II presents the calculated splitting for the $^5I_4$ and $^5I_5$ multiplet manifolds of Pm^{3+} using as a starting set of B_{nm}, the parameters for Sm^{3+} in AlN listed in Table III corrected to Pm^{3+} through the three-parameter theory developed by Morrison *et al.*[35,36] The calculated splitting for $^5F_1$ is 11 945 cm^{-1} and 11 919 cm^{-1}, in good agreement with the experimental levels chosen as the emitting levels (see Table II). A total of 15 experimental Stark levels from $^5I_4$, $^5I_5$, and $^5F_1$ were modeled for the crystal-field splitting of the manifolds, and a rms deviation of 7 cm^{-1} was obtained from a least-squares fitting analysis. The resulting six phenomenological parameters B_{nm} (C_{3v} symmetry) are listed in Table III.

VI. LIFETIME MEASUREMENTS

Figure 10 shows the temperature-dependent lifetime of the initial $^4G_{5/2}$ multiplet manifold of Sm^{3+}. The lifetime was determined by monitoring the $^4G_{5/2} \rightarrow {}^6H_{9/2}$ transition around 673 nm. The experimental luminescence decay was fitted towards a single exponential decay curve. The observed lifetime increases from about 0.71 μs at 12 K to 0.8 μs at 300 K. This is in contrast to the behavior observed by

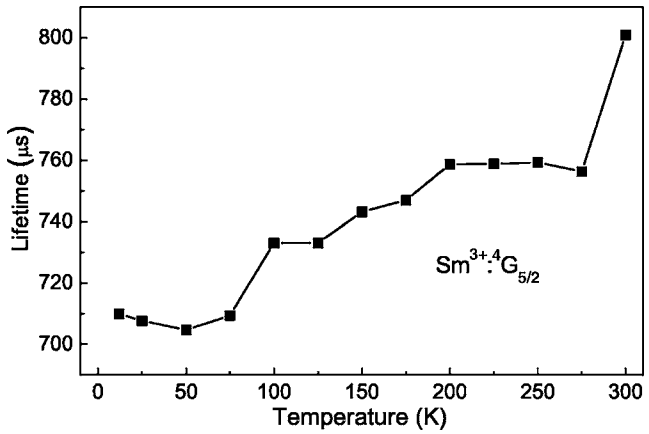

FIG. 10. Temperature-dependent lifetime of the $^4G_{5/2}$ level of Sm^{3+} in *w*-AlN, measured at the $^4G_{5/2} \rightarrow {}^6H_{9/2}$ transition around 673 nm.

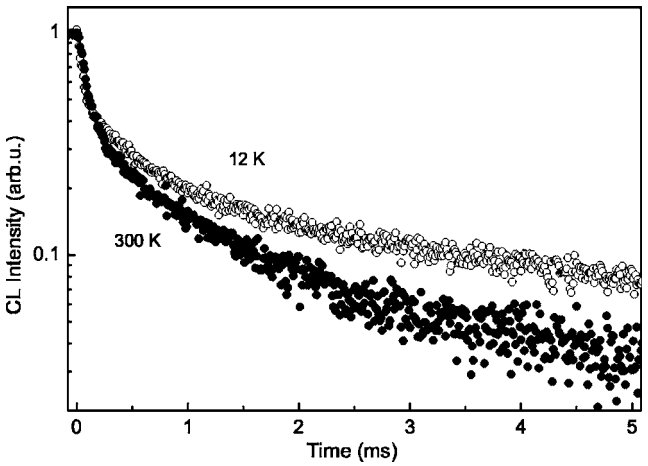

FIG. 11. Initial part of the decay curve of the $^5F_1$ level of Pm^{3+}, measured at the $^5F_1 \rightarrow {}^5I_4$ transition around 840 nm, shown for temperatures 12 K and 300 K. The background was substracted from the spectra.

Gruber *et al.*[16] in the case of Sm^{3+} in GaN, where an increase in lifetime of the $^4G_{5/2}$ manifold by a factor of two was observed in this temperature range.

In the case of Pm^{3+} the lifetime of the initial $^5F_1$ manifold was monitored at the $^5F_1 \rightarrow {}^5I_4$ transition around 840 nm. Fitting of the decay curve was not possible in this case, because neither a single or double exponential behavior nor a decay of the Inokuti-Hirajama[37] type could, at least consistently through the whole temperature range, reasonably describe the decay. Figure 11 shows the initial part of the decay curve of the $^5F_1$ multiplet at 12 K and at 300 K; the background was properly substracted. In the beginning, the luminescence rapidly decreases with a lifetime of 50–100 μs, while the later part shows a slower lifetime of more than 1 ms. For a summary of lifetimes of Pm^{3+} in different hosts, see Ref. 31. It is interesting to note that the $^5F_2$ manifold of Pm^{3+}, typically located about 400 cm^{-1} above the $^5F_1$ level, is neither visible in the survey or high-resolution CL spectra, nor is there any signature in the decay of the $^5F_1$ level itself. Both levels must therefore be treated as coupled, even for low temperatures. Finally we note that there was no direct evidence of energy transfer between Sm^{3+} and Pm^{3+} ions in the decay spectra, at least for the initial multiplet manifolds under investigation.

VII. SUMMARY OF RESULTS

In summary, we present lattice location studies of ^{147}Nd and ^{147}Pm in *w*-AlN in combination with crystal-field splitting analyses of some of the energy levels of $^{147}Pm^{3+}$ and $^{147}Sm^{3+}$ including lifetime measurements of the dominant multiplet manifolds. The crystal-field analysis is based on the splitting of individual $^{2S+1}L_J$ multiplet manifolds by a crystalline field whose parameters B_{nm} are determined from lattice sum calculations that assume the Pm^{3+} and Sm^{3+} ions replace the Al^{3+} site in the AlN lattice, which is confirmed by the lattice location studies as the dominant lattice site. For

the crystal-field analysis we furthermore assume that this substitutional Al lattice site is of C_{3v} symmetry. Emitting Stark levels from the $^4G_{5/2}$ manifolds of Sm^{3+} establish the splitting of the $^6H_{5/2,7/2,9/2,11/2,13/2,15/2}$ and $^6F_{1/2,5/2}$ manifolds for this ion based on an energy-difference analysis of 31 Stark levels. In the case of Pm^{3+} transitions between individual Stark levels of the emitting $^5F_1$ manifold and the terminal manifolds $^5I_4$ and $^5I_5$ are observed and compared to a splitting based on B_{nm} parameters that are directly obtained on the basis of the B_{nm} parameters derived for Sm^{3+} in AlN in this work. In the case of Pm^{3+} transitions between individual Stark levels are accompanied by a large number of weak sidebands, which makes the crystal-field analysis difficult.

*Present address: Philipps-Universität Marburg, Fachbereich Physik, Renthof 5, D-35032 Marburg, Germany.

[1] J. D. MacKenzie, C. R. Abernathy, S. J. Pearton, U. Hommerich, X. Wu, R. N. Schwartz, R. G. Wilson, and J. M. Zavada, Appl. Phys. Lett. **69**, 2083 (1996).
[2] J. D. MacKenzie, C. R. Abernathy, S. J. Pearton, U. Hommerich, X. Wu, R. N. Schwartz, R. G. Wilson, and J. M. Zavada, J. Cryst. Growth **175**, 84 (1997).
[3] W. M. Jadwisienczak, H. J. Lozykowski, I. Berishev, A. Bensaoula, and I. G. Brown, J. Appl. Phys. **89**, 4384 (2001).
[4] M. L. Caldwell, P. G. Van Patten, M. E. Kordesch, and H. H. Richardson, MRS Internet J. Nitride Semicond. Res. **6**, 1 (2001).
[5] U. Vetter, J. Zenneck, and H. Hofsäss, Appl. Phys. Lett. **83**, 2145 (2003).
[6] H. J. Lozykowski, W. M. Jadwisienczak, A. Bensaoula, and O. Monteiro, Microelectron. J. **36**, 453 (2005).
[7] S. W. Choi, S. Emura, S. Kimura, M. S. Kim, Y. K. Zhou, N. Teraguchi, A. Suzuki, A. Yanase, and H. Asahi, J. Alloys Compd. **408**, 717 (2006).
[8] U. Vetter, M. F. Reid, H. Hofsäss, C. Ronning, J. Zenneck, M. Dietrich, and the ISOLDE Collaboration, Mater. Res. Soc. Symp. Proc. **743**, L6.16 (2003).
[9] C. J. Ellis, R. M. Mair, J. Li, J. Y. Lin, H. X. Jiang, J. M. Zavada, and R. G. Wilson, Mater. Sci. Eng., B **81**, 167 (2001).
[10] C. W. Lee and A. J. Steckl, Appl. Phys. Lett. **83**, 2094 (2003).
[11] U. Vetter, H. Hofsäss, and T. Taniguchi, Appl. Phys. Lett. **84**, 4286 (2004).
[12] U. Vetter, P. Reinke, C. Ronning, H. Hofsäss, P. Schaaf, K. Bharuth-Ram, and T. Taniguchi, Diamond Relat. Mater. **12**, 1182 (2003).
[13] A. Nakayama, T. Taniguchi, Y. Kubota, K. Watanabe, S. Hishita, and H. Kanda, Appl. Phys. Lett. **87**, 211913 (2005).
[14] D. E. Nazyrov, G. S. Kulikov, and R. S. Malkovich, Tech. Phys. Lett. **23**, 68 (1997).
[15] W. T. Carnall, H. Crosswhite, H. M. Crosswhite, and J. G. Conway, J. Chem. Phys. **64**, 3582 (1976).
[16] J. B. Gruber, B. Zandi, H. J. Lozykowski, and W. M. Jadwisienczak, J. Appl. Phys. **91**, 2929 (2002).
[17] E. Kugler, Hyperfine Interact. **129**, 23 (2000).
[18] R. B. Firestone, *Table of Isotopes*, 8th ed. (John Wiley & Sons, Inc., New York, 1996).
[19] H. Hofsäss, Hyperfine Interact. **97/98**, 247 (1996).
[20] H. Hofsäss and G. Lindner, Phys. Rep. **201**, 121 (1991).
[21] U. Wahl, J. G. Correia, S. Cardoso, J. G. Marques, A. Vantomme, and G. Langouche, Nucl. Instrum. Methods Phys. Res. B **137**, 744 (1998).
[22] U. Wahl, J. G. Correia, A. Czermak, S. G. Jahn, P. Jalocha, J. G. Marques, A. Rudge, F. Schopper, J. C. Soares, A. Vantomme, and P. Weilhammer, Nucl. Instrum. Methods Phys. Res. A **524**, 245 (2004).
[23] U. Wahl, J. G. Correia, E. Rita, E. Alves, J. C. Soares, B. De Vries, V. Matias, and A. Vantomme, Hyperfine Interact. **159**, 363 (2004).
[24] S. J. Rhee, S. Kim, W. S. Sterner, J. O. White, and S. G. Bishop, J. Appl. Phys. **90**, 2760 (2001).
[25] J. B. Gruber, U. Vetter, H. Hofsäss, B. Zandi, and M. F. Reid, Phys. Rev. B **70**, 245108 (2004).
[26] J. B. Gruber, U. Vetter, H. Hofsäss, B. Zandi, and M. F. Reid, Phys. Rev. B **69**, 195202 (2004).
[27] B. De Vries, A. Vantomme, U. Wahl, S. Ruffenach, O. Briot, J. G. Correia, and the ISOLDE Collaboration (unpublished).
[28] G. Öhl, U. Vetter, and H. Hofsäss (unpublished).
[29] S. Petit, R. Jones, M. J. Shaw, P. R. Briddon, B. Hourahine, and T. Frauenheim, Phys. Rev. B **72**, 073205 (2005).
[30] C. A. Morrison and R. P. Leavitt, in *Handbook on the Physics and Chemistry of Rare Earths*, edited by K. A. Gscheidner, Jr. and L. Eyring (North-Holland Publishing Company, Amsterdam, 1982), p. 461.
[31] M. D. Shinn, W. F. Krupke, W. R. Solarz, and T. A. Kirchoff, IEEE J. Quantum Electron. **24**, 1100 (1988).
[32] W. Baer, J. G. Conway, and S. P. Davis, J. Chem. Phys. **59**, 2294 (1973).
[33] J. B. Gruber, B. Zandi, H. J. Lozykowski, W. M. Jadwisienczak, and I. Brown, J. Appl. Phys. **89**, 7973 (2001).
[34] J. B. Gruber, B. Zandi, H. J. Lozykowski, and W. M. Jadwisienczak, J. Appl. Phys. **92**, 5127 (2002).
[35] C. A. Morrison and R. P. Leavitt, J. Chem. Phys. **71**, 2366 (1979).
[36] C. A. Morrison, R. P. Leavitt, and D. E. Wortman, J. Chem. Phys. **73**, 2580 (1980).
[37] M. Inokuti and F. Hirayama, J. Chem. Phys. **43**, 1978 (1965).